

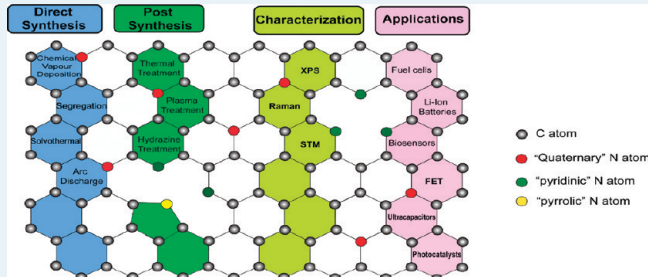
Review on Recent Progress in Nitrogen-Doped Graphene: Synthesis, Characterization, and Its Potential Applications

Haibo Wang, Thandavarayan Maiyalagan, and Xin Wang*

School of Chemical and Biomedical Engineering, Nanyang Technological University, 62 Nanyang Drive, Singapore, 637459

ABSTRACT: Nitrogen doping has been an effective way to tailor the properties of graphene and render its potential use for various applications. Three common bonding configurations are normally obtained when doing nitrogen into the graphene: pyridinic N, pyrrolic N, and graphitic N. This paper reviews nitrogen-doped graphene, including various synthesis methods to introduce N doping and various characterization techniques for the examination of various N bonding configurations. Potential applications of N-graphene are also reviewed on the basis of experimental and theoretical studies.

KEYWORDS: graphene, nitrogen doping, electrocatalysis, field-effect transistor, energy storage



1. INTRODUCTION

Graphene is a novel nanomaterial with a single sheet of carbon atoms packed in a hexagonal lattice. Since the first report of its synthesis via a “Scotch tape” method in 2004,¹ graphene has emerged as one of the most active research fields. The fascinating properties of graphene, such as a high surface area (2630 m²/g),² high thermal conductivity (~5000 W/mK),³ fast charged carrier mobility (~200 000 cm² V⁻¹ s⁻¹)³ and strong Young’s modulus (~1 TPa),⁴ have been well documented. Various morphologies have also been obtained, including two-dimensional graphene nanosheets (GNSSs), one-dimensional graphene nanoribbons (GNRs),^{5–7} and zero-dimensional graphene quantum dots.^{8,9} Their properties can also be tuned by their size and edges. For instance, GNRs with width narrower than 10 nm showed obvious semiconducting characteristics, but GNRs with width larger than 10 nm exhibited very weak gate dependence.¹⁰ The increased concentration of a zigzag edge tended to decrease its band gap.⁹ All these aspects make graphene material promising for various applications, including energy conversion and storage, electrocatalysis, sensors and electronics.

Other than morphology control, chemical doping is another important approach to tailor the property of graphene, which has been proved effective in the doping of carbon nanotubes (CNTs) and greatly broadened their applications.^{11–15} Usually, there are two means to chemically dope graphene: (1) the adsorption of gas,¹⁶ metal,¹⁷ or organic molecules¹⁸ to the graphene surface and (2) substitutional doping, which introduces heteroatoms, such as nitrogen atoms and boron atoms, into the carbon lattice of graphene. Both of these methods can modulate the electronic properties of graphene. In this paper, our focus will be constrained to the topic of nitrogen-doped graphene (N-graphene).

When a nitrogen atom is doped into graphene, it usually has three common bonding configurations within the carbon

lattice, including quaternary N (or graphitic N), pyridinic N, and pyrrolic N (Figure 1). Specifically, pyridinic N bonds with

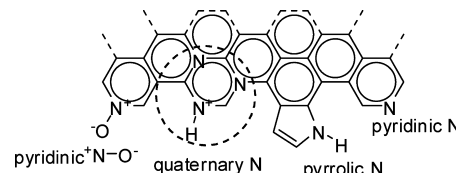


Figure 1. Bonding configurations for nitrogen atoms in N-graphene.²⁴

two C atoms at the edges or defects of graphene and contributes one p electron to the π system. Pyrrolic N refers to N atoms that contribute two p electrons to the π system, although unnecessarily bond into the five-membered ring, as in pyrrole.^{19,20} Quaternary N refers to N atoms that substitute for C atoms in the hexagonal ring. Among these nitrogen types, pyridinic N and quaternary N are sp^2 hybridized and pyrrolic N is sp^3 hybridized. Apart from these three common nitrogen types, N oxides of pyridinic N have been observed in both the N-graphene and N-CNT studies.^{21–23} In this configuration, the nitrogen atom bonds with two carbon atoms and one oxygen atom.

The N-graphene shows different properties compared with the pristine graphene. For instance, the spin density and charge distribution of carbon atoms will be influenced by the neighbor nitrogen dopants,^{25,26} which induces the “activation region” on the graphene surface. This kind of activated region can participate in catalytic reactions directly, such as the oxygen

Special Issue: Electrocatalysis

Received: December 12, 2011

Revised: February 23, 2012

Table 1. Nitrogen-Doping Methods and Nitrogen Concentration on Graphene

no.	synthesis method	precursors	N content, at. %	application/reference
1	CVD	Cu film on Si substrate as catalyst, CH ₄ /NH ₃	1.2–8.9	FET ³⁰
2	CVD	Cu foil as catalyst, NH ₃ /He	1.6–16	ORR ⁴⁰
3	CVD	Ni film on SiO ₂ /Si substrate as catalyst, NH ₃ /CH ₄ /H ₂ /Ar (10:50:65:200)	4	ORR ⁴¹
4	CVD	Cu foil as catalyst, acetonitrile	~9	lithium battery ⁴³
5	CVD	Cu foil as catalyst, pyridine	~2.4	FET ⁴⁴
6	segregation growth	carbon-contained Ni layer on nitrogen-contained boron layer	0.3–2.9	FET ⁵⁰
7	solvothermal	Li ₃ N/CCl ₄ (NG1) or N ₃ C ₃ Cl ₃ /Li ₃ N/CCl ₄ (NG2)	4.5 (NG1) or 16.4 (NG2)	ORR ⁵²
8	arc discharge	graphite/H ₂ /He/pyridine (NG1) graphite/H ₂ /He/NH ₃ (NG2) transformation of nanodiamond/He/pyridine (NG3)	0.6 (NG1), 1 (NG2), 1.4 (NG3)	56, 57
9	thermal treatment	N ⁺ ion-irradiated graphene, NH ₃	1.1	FET ⁵⁹
10	thermal treatment	graphite oxide after thermal expansion, NH ₃ /Ar	2.0–2.8	ORR ⁶⁰
11	thermal treatment	GNR, NH ₃		FET ³¹
12	thermal treatment	GO, NH ₃ /Ar (10% NH ₃)	~3–5	FET ⁶³
13	thermal treatment	GO, NH ₃	6.7–10.78	methanol oxidation ⁷³
14	thermal treatment	GO, melamine	7.1–10.1	ORR ⁶²
15	plasma treatment	graphite oxide after thermal expansion, N ₂ plasma	8.5	ORR ²³
16	plasma treatment	graphite oxide after thermal expansion, N ₂ plasma	3	ORR ⁶⁷
17	plasma treatment	chemically synthesized graphene, N ₂ plasma	~1.3	biosensors ⁶⁸
18	plasma treatment	GO, treat with H ₂ plasma first, then treat with N ₂ plasma	1.68–2.51	ultracapacitor ⁶⁹
19	plasma treatment	mechanically exfoliated graphene or bilayer graphene grown by CVD, NH ₃ plasma		FET ⁷⁰
20	N ₂ H ₄ treatment	GO, N ₂ H ₄ , NH ₃	4.01–5.21	71
21	N ₂ H ₄ treatment	graphite oxide after thermal expansion, N ₂ H ₄	1.04	electrochemical sensor ⁷²

70 reduction reaction (ORR), or anchor the metal nanoparticles
71 used in the catalytic reaction. Moreover, after nitrogen doping
72 in the monolayer graphene, the Fermi level shifts above the
73 Dirac point,^{27,28} and the density of state near the Fermi level is
74 suppressed;^{29,30} thus, the band gap between the conduction
75 band and the valence band will be opened. For GNRs, the band
76 gap is still kept after doping.³¹ The band gap in N-graphene
77 makes it a candidate to be used in semiconductor devices. Apart
78 from these, N-graphene can also be used in batteries, sensors,
79 and ultracapacitors. The nitrogen doping of graphene greatly
80 broadens its applications.

81 Previously, several reviews on graphene have mentioned N-
82 graphene,^{32–35} especially the review of Liu et al.,³⁵ which
83 focused on two chemical doping approaches and band gap
84 tuning; however, there is still no systematical study of N-
85 graphene synthesized by substitutional doping. Therefore, in
86 this review, we summarize different synthesis and character-
87 ization methods of nitrogen-substituted graphene; the
88 application of N-graphene is also reviewed on the basis of
89 experimental and theoretical studies.

2. SYNTHESIS OF N-GRAFENE

90 Similar to the synthesis of N-CNT, N-graphene can be
91 obtained through two different ways: direct synthesis and
92 post treatment. Most postsynthesis treatments may lead to
93 surface doping only. Although in principle, direct synthesis may

have the potential to create a homogeneous doping throughout
94 the bulk material, the results reported so far fail to indicate so.
95 Specifically, direct synthesis includes chemical vapor deposition
96 (CVD), segregation growth, solvothermal, and arc-discharge
97 approaches. Post treatment includes thermal treatment, plasma
98 treatment, and N₂H₄ treatment. Table 1 gives a summary of
99 various methods used for the synthesis of N-graphene. Detailed
100 discussion on these methods is elaborated below.
101

102 **2.1.1. Direct Synthesis. CVD Approach.** CVD is a widely
103 used method to synthesize various carbon nanomaterials, such as
104 graphene,³⁶ CNTs,³⁷ carbon nanofibers,³⁸ and N-doped
105 CNTs.³⁹ Recently, it was successfully applied to prepare N-
106 graphene. Typically,^{30,40,41} a metal catalyst (Cu or Ni) is used
107 as the substrate, then at high temperature, a carbon source gas
108 mixed with a nitrogen-containing gas is introduced. These
109 precursors dissociate and recombine into N-graphene by means
110 of precipitation on the surface of the catalyst.^{30,42}

111 Apart from the gas mixture, liquid organic precursors
112 (acetonitrile, pyridine) have also been used to form N-
113 graphene.^{43,44} Theoretical study about different precursors⁴⁵
114 shows that proper skeletal bonds of liquid precursors are crucial
115 for the formation of N-graphene. Acrylonitrile containing the
116 C–C single bond, C=C double bond, and C≡N triple bond
117 cannot form N-graphene, but pyridine with only the double
118 bond forms N-graphene. The proposed reason is that the single
119 bond is easy to break, even at low temperature, leaving C=C
120 and C≡N bonds at the catalyst surface. Then C≡N bond is

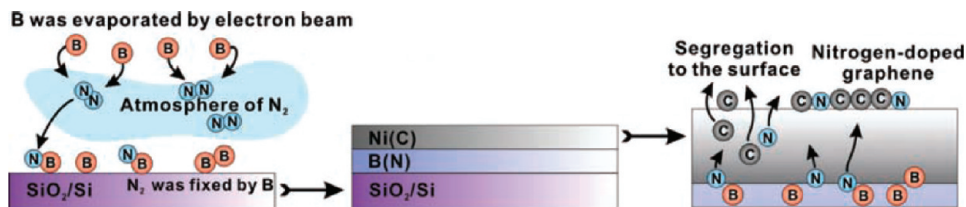


Figure 2. Schematic illustration of the segregation technique for growing N-doped graphene.⁵⁰

preferentially removed from the surface by forming volatile molecules when the temperature is higher than 400 °C; thus, only C=C will be left to form nondoped graphene above 500 °C. In contrast, the skeletal bonds in pyridine have similar bond energies, which induces the formation of N-graphene.

The layer distribution of N-graphene is varied in different studies. Although the N-graphene synthesized from the gas mixture C₂H₄/NH₃ is claimed to be monolayer through the analysis of Raman spectroscopy,⁴⁰ N-graphene synthesized from a gas mixture, CH₄/NH₃,^{30,41} shows that the few-layer graphene is predominant after high-resolution transmission electron microscope (HRTEM) characterization. In other studies, monolayer N-graphene is also obtained when acetonitrile⁴³ or pyridine⁴⁴ is used as precursors. Furthermore, the layer of N-graphene can be adjusted by the flowing time if acetonitrile is used as the precursor.⁴³

In the CVD approach, the nitrogen content can be controlled by changing the flow rate⁴⁰ and the ratio between carbon source and nitrogen source.³⁰ It has been reported³⁰ that the doping level decreased from 8.9 to 3.2 or 1.2 at. % if the NH₃/CH₄ ratio was lowered from 1:1 to 1:2 or 1:4, respectively. Moreover, although high nitrogen content (~16 at. %) has been reported,⁴⁰ the nitrogen content in this method is normally around 4–9 at. %.

The bonding configuration of nitrogen within N-graphene varies with different studies. By using Cu as the catalyst and CH₄/NH₃ (1:1) as the precursor, the nitrogen type in N-graphene is mainly quaternary N;³⁰ however, when Ni is used as the catalyst and CH₄/NH₃ (5:1) is used as the precursor, the N-graphene obtained consists of mainly pyridinic N and pyrrolic N.⁴¹ If C₂H₄/NH₃ is used as the precursor while keeping Cu as the catalyst, the pyridinic N becomes the predominant type.⁴⁰ Notably, the syntheses of other nitrogen-doped carbon materials have revealed that the doping environment is also influenced by the flow rate, catalyst, and growth temperature,^{46–49} so further research is required to clarify the relationship between the bonding configuration of nitrogen and the parameters of CVD.

2.1.2. Segregation Growth Approach. In this approach, a nitrogen-containing boron layers and carbon-containing nickel layers are sequentially deposited on the SiO₂/Si substrate by electron beam evaporation, then during the vacuum annealing process, the boron atoms are trapped by nickel, and the carbon atoms will segregate out onto the nickel surface and combine to form N-graphene (Figure 2).⁵⁰ Although sporadic multilayer areas are observed, the N-graphene generally shows a large-scale, uniform, and few-layer structure. The nitrogen content (0.3–2.9 at. %) can be controlled by adjusting the thickness of the boron and nickel films. The pyridinic and pyrrolic N are dominant in N-graphene. Interestingly, the graphene can be doped in a specific area by embedding nitrogen species into the selective area of the substrate.

2.1.3. Solvothermal Approach. The solvothermal approach was first employed for gram-scale production of graphene.⁵¹ Recently, gram-scale production of N-graphene has been achieved by applying this approach at ~300 °C. By mixing lithium nitride (Li₃N) with tetrachloromethane (CCl₄) (Figure 3) or cyanuric chloride (N₃C₃Cl₃) with Li₃N and CCl₄, N-

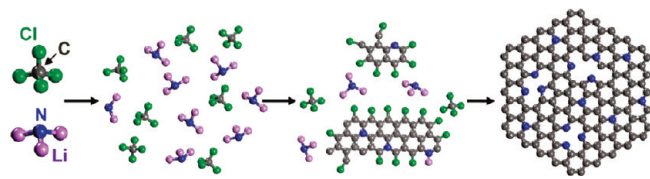


Figure 3. Schematic illustration for N-graphene synthesized from the reaction of CCl₄ and Li₃N.⁵²

graphene with different nitrogen contents was obtained (denoted as NG1 and NG2, respectively).⁵² The HRTEM images of N-graphene show that it mainly consists of 1–6 layer graphene. Because of the introduction of N₃C₃Cl₃, NG2 has a higher nitrogen content (16.4 at. %) compared with NG1 (4.5 at. %). The proportion of doped nitrogen species also changes with different reactant mixtures. The quaternary N dominates in NG1, and pyridinic and pyrrolic N dominates in NG2.

2.1.4. Arc-Discharge Approach. An arc-discharge approach has been applied to obtain CNTs and doped CNTs by evaporating the carbon source, normally graphite,^{53–55} at high temperature. Rao et al.^{56,57} successfully obtained N-graphene by applying this method in the presence of pyridine vapor or NH₃. The N-graphene synthesized from transformation of nanodiamond shows higher nitrogen content than that synthesized from graphite. The nitrogen content of the as-synthesized N-graphene is around 0.5–1.5 at. %. Moreover, although single layer N-graphene is occasionally observed, most of the N-graphene possesses two or three layers. The scale of graphene and N-graphene produced by this method normally is below 1 μm.^{56,58}

2.2.1. Postsynthesis Treatment. Thermal Treatment. Thermal treatment refers to the method using high temperature to produce N-graphene. It has been shown that heating graphene in NH₃ at high temperature (≥800 °C) can produce N-graphene.^{59,60} Electrical annealing, which produces high temperature, has also been applied to obtain N-GNRs.³¹ The nitrogen content in the N-graphene synthesized by this method is relatively low. Guo et al.⁵⁹ obtained N-graphene with 1.1 at. % doping level at 1100 °C; Geng et al.⁶⁰ reported that the highest nitrogen content was 2.8 at. % at 800 and 900 °C. The low doping level may be attributed to two reasons: one is the insufficient defect number in the high quality graphene, and the other is the high annealing temperature, which will break the C–N bonds in N-graphene.⁶¹ Moreover, the nitrogen doping is more likely to occur at the defects and edge of graphene in the thermal treatment method. Geng et al.⁶⁰ found pyridinic and

216 pyrrolic N dominated in the N-graphene. Wang et al.³¹ claimed
217 that nitrogen atoms preferred functionalizing the edge of
218 GNRs. Interestingly, unlike NH₃, annealing N⁺ ion irradiated
219 graphene in N₂ at high temperature cannot introduce nitrogen
220 into the graphene,⁵⁹ which suggests that the inertness of N₂
221 makes it difficult to react with the reactive carbon atoms on the
222 defect sites in graphene.

223 Apart from graphene, graphene oxide can also be used to
224 synthesize N-graphene by thermal treatment in the presence of
225 various nitrogen precursors. Sheng et al.⁶² reported that
226 annealing GO in the presence of melamine at high temperature
227 (700–1000 °C) could produce N-graphene. The layer
228 distribution of N-graphene depends on the synthesis procedure.
229 Few-layer N-graphene is obtained if annealing the mixture of
230 GO and melamine at high temperature, and single layer N-
231 graphene can be produced if heating single-layer GO covered
232 with melamine. The nitrogen content is affected by both the
233 temperature and the mass ratio between GO and melamine.
234 The largest nitrogen content (10.1 at. %) is obtained under 700
235 °C when the mass ratio of GO to melamine is 0.2. Li et al.⁶³
236 showed that placing GO in an NH₃ atmosphere through
237 thermal annealing (500 °C) could reduce GO and get N-
238 graphene with a 5 at. % nitrogen doping level. Notably, both of
239 these works report that the temperature has the major influence
240 on the nitrogen content of N-graphene. Li et al.⁶³ ascribed the
241 reason to the decreased content of oxygen functional groups at
242 higher temperature. Because these oxygen functional groups are
243 responsible for the formation of a C–N bond, the reactivity
244 between GO and nitrogen atoms will decrease after these
245 groups decompose at higher temperature, resulting in the lower
246 nitrogen content. Moreover, it has been claimed that lowering
247 the mass ratio between GO and melamine at 800 °C induced
248 higher nitrogen doping level, which may suggest the
249 competitive doping between oxygen and melamine.⁶²

250 **2.2.2. Plasma Treatment.** When carbon material is placed in
251 the nitrogen plasma atmosphere, carbon atoms will be partly
252 replaced by nitrogen atoms; therefore, this method was applied
253 to synthesize N-CNTs.^{64–66} Recently, it has been reported that
254 N-graphene could be prepared from graphene^{23,67,68} or GO⁶⁹
255 by exposing it to the nitrogen plasma. NH₃ plasma has also
256 been used to obtain N-graphene from mechanically exfoliated
257 graphene.⁷⁰ The nitrogen content, which can be controlled by
258 the plasma strength and exposure time, varies from 3 to 8.5 at.
259 % in different works. During the plasma exposure process,
260 defects and oxygen-containing groups are created^{23,68} Shao et
261 al.²³ showed that graphene contains 3.5 at. % oxygen species
262 while the N-graphene contains 8.6 at. % oxygen species, Wang
263 et al.⁶⁸ reported that the content of oxygen species increased
264 from about 15 to 26–28 at. % after doping. These results
265 indicate the plasma treatment introduces a significant amount
266 of oxygen species into graphene. The reason may be ascribed to
267 the reactive carbon atoms at the edge of defects that are created
268 by the plasma treatment.²³ Notably, in the N₂ plasma
269 treatment, overexposure may decrease the electrocatalytic
270 activity of N-graphene.⁶⁸ It has been reported that if graphene
271 was exposed to the N₂ plasma over 40 min, the reduction
272 current of H₂O₂ would decrease because of the destruction and
273 split of the graphene plane.

274 **2.2.3. Hydrazine Hydrate (N₂H₄) Treatment.** Using
275 hydrazine hydrate to prepare graphene from GO is a widely
276 used method. Recently, N-graphene has been obtained by
277 reducing GO in the NH₃ and N₂H₄ mixed solution.⁷¹ The
278 nitrogen content reaches up to 5 at. % when the reduction

279 temperature is 80 °C; however, the absorbed N₂H₄ takes a non-
280 negligible proportion in the total nitrogen content. If the
281 reaction temperature rises to 160 °C or higher, the N₂H₄ will
282 be desorbed and the nitrogen content decreases to ~4 at. %.
283 Interestingly, the morphology of N-graphene also changes with
284 the temperature. The relative flat N-graphene is generated if
285 GO is reduced at low temperature (\leq 120 °C), whereas the
286 obvious agglomeration in N-graphene will occur if the
287 temperature is higher.
288

289 By using ultrasonication,⁷² N-graphene can be synthesized
290 from graphene in the presence of N₂H₄. The agglomerated
291 regions are also observed after doping. The nitrogen content is
292 around 1 at. %. In addition to these, the nitrogen species in the
293 N-graphene contains only pyridonic and pyrrolic nitrogen. The
294 content and bonding configuration of nitrogen indicates the
295 nitrogen atoms can be introduced only to the graphene edges
296 and defects in this method.
297

3. CHARACTERIZATION TECHNIQUES FOR STUDYING NITROGEN-DOPED GRAPHENE

298 **3.1. X-ray Photoelectron Spectroscopy (XPS) Technique.** XPS is the standard technique to study the nitrogen-
299 doping effect in graphene. In the XPS spectrum of N-graphene,
300 the peaks appearing at about 400 and 284 eV correspond to the
301 N1s and C1s, respectively. The ratio of peak intensity between
302 N1s and C1s is used to determine the nitrogen content in N-
303 graphene. Moreover, the N1s spectrum is used to determine
304 the nitrogen configurations. In the research about N-graphene,
305 the N1s spectrum usually can be deconvoluted to several
306 individual peaks that are assigned to pyridinic N (398.1–399.3
307 eV), pyrrolic N (399.8–401.2 eV), and quaternary N (401.1–
308 402.7 eV) (Figure 4). The peak position of these nitrogen types
309 f4

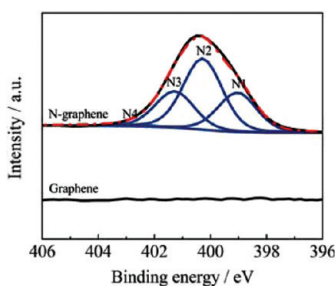


Figure 4. High-resolution N1s XPS spectra of graphene and N-graphene. N1 represents pyridinic N, N2 represents pyrrolic N, N3 represents quaternary N, and N4 represents the N-oxides of pyridinic N.²³

310 varies in a relatively wide range in different studies. Reddy et
311 al.⁴³ reported the pyrrolic N appeared at 401.2 eV, whereas Li
312 et al.⁶³ showed the quaternary N appeared at about 401.1 eV.
313 The large difference of the peak positions of nitrogen
314 configurations may be due to the different environments of
315 nitrogen.¹⁹ The charge of nitrogen and its neighbor atoms and
316 the electron redistribution after ionization will all influence the
317 precise position of different nitrogen types. Apart from these
318 three nitrogen types, peak corresponding to N-oxides of
319 pyridinic N is observed at ~402.8 eV in several studies.^{23,62}

320 When nitrogen atoms are doped into graphene, peaks at the
321 C1s spectrum will change accordingly.^{50,62,63,70,71} In the C1s
322 spectrum of GO (Figure 5a), the sharp peak at around 284.5 eV
323 corresponds to the sp² carbon with C=C bonds. Another
324 strong peak at higher energy corresponds to the sp³ carbon
325

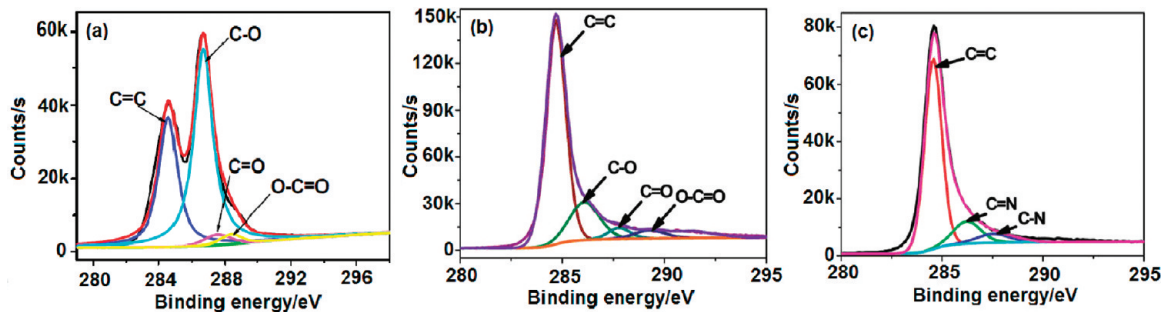


Figure 5. High-resolution C1s spectra of the (a) GO, (b) graphene prepared by annealing GO in Ar at 800 °C, and (c) N-graphene prepared by annealing GO/melamine (1:5) at 800 °C for 30 min.⁶²

with several different C–O bonding configurations. These configurations include the C–O bonds, carbonyls (C=O), and carboxylates (O=C–O) at about 286.2, 287.8, and 289.2 eV, respectively. After GO is annealed in Ar, the intensity of the peak ascribed to the C–O bonding configurations decreases to a much lower value (Figure 5b).⁶² This indicates that most of the oxygen groups in GO are removed after annealing. If GO is doped with nitrogen atoms (Figure 5c), peaks ascribed to C–O bonding configurations disappear, and new small peaks appear after peak fitting.^{50,62,70,71} In the work of Sheng et al.,⁶² new peaks appearing at 285.8 and 287.5 eV were assigned to the sp^2 and sp^3 carbon atoms, respectively. In other works,^{50,70} a new small peak at ~289 eV was observed. This peak is ascribed to the physisorbed oxygen on the graphene. Generally speaking, the peak change at higher energy in the C1s spectrum suggests the nitrogen doping occurs in the graphene.

3.2. Raman Spectroscopy. Raman spectroscopy is another very useful method to characterize N-graphene. The D, G, and 2D bands are the predominant features in the spectrum of N-graphene. They are represented by peaks at around 1320–1350, 1570–1585, and 2640–2680 cm^{-1} , respectively (Figure 6.) In some studies,^{40,52} the peak called D' will appear at

and one defect for the D mode. Different from the D band which requires defects to activate it, the 2D band does not require the activation of defects. Thus, the 2D band is always seen in the Raman spectra of graphene and N-graphene, even when the D band cannot be observed. For the D' band, it arises from the intravalley, defect-induced, double-resonance process.

Previous studies^{77,79} have revealed that the intensity ratio of the D and G bands (I_D/I_G) was inversely proportional to the in-plane crystallite sizes L_a . The crystallite size can be determined according to the Tuinstra–Koenig (TK) relation, $L_a(\text{nm}) = (2.4 \times 10^{-10}) \lambda^4 (I_D/I_G)^{-1}$ (λ is the Raman excitation wavelength). For nitrogen doping, the substitution of nitrogen atoms usually is accompanied by the introduction of defects into the graphene surface. Considering L_a as the average interdefect distance, more defects undoubtedly means a smaller L_a ; thus, L_a can be used to study defects introduced by nitrogen doping. Comparing the crystallite size of pristine graphene with N-graphene, Zhang et al.⁵⁰ reported that the I_D/I_G of graphene and N-graphene with lower (NG1) and higher (NG2) nitrogen doping level are 0.26, 0.8 and 2.1, which corresponds to crystallite sizes of 65, 21, and 8 nm, respectively (Figure 7).

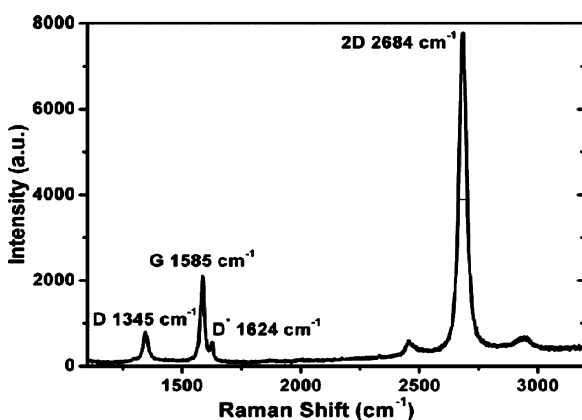


Figure 6. Typical Raman spectrum of N-graphene transferred onto a SiO_2/Si substrate. The laser excitation wavelength is 514.5 nm.⁴⁴

~1602–1625 cm^{-1} . These bands already have been studied intensively in former studies.^{74–78} Specifically, the G band corresponds to the doubly degenerate E_{2g} phonons at the Brillouin zone. It originates from the first-order Raman scattering process. The 2D and D bands are all induced by the second-order, double-resonance process and related to zone-boundary phonons. The scattering process involves two zone-boundary phonons for 2D mode; it involves one phonon

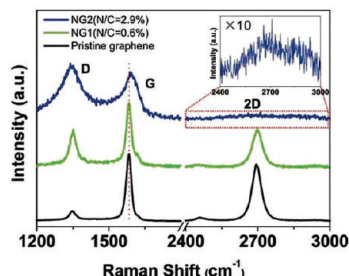


Figure 7. Raman spectra of pristine graphene and N-graphene with 0.6 (NG1) and 2.9 (NG2) at % doping level. The inset shows the enlarged 2D band of NG2. The laser excitation wavelength is 514.5 nm.⁵⁰

This suggests the crystallite size decreases remarkably with an increase in the nitrogen doping level because of the defects.

Apart from I_D/I_G , the intensity ratio of the 2D and G bands (I_{2D}/I_G) has been used to characterize N-graphene. It has been reported that I_{2D}/I_G depends on the electron concentration (Figure 8).⁸⁰ The G band always stiffens, and the 2D band responds differently to hole and electron doping; thus, I_{2D}/I_G has been used to estimate the nitrogen doping level.^{50,70} Through calculating the I_{2D}/I_G , which was <0.6 in N-graphene, it was concluded that the doping level was higher than $4 \times 10^{13} \text{ cm}^{-2}$. Notably, some studies also presented that the G band increased almost linearly, corresponding to the increment of

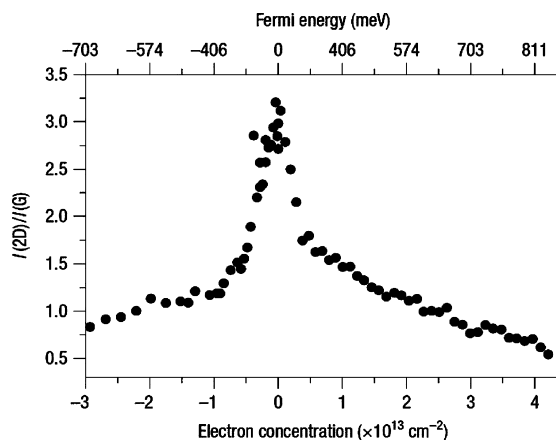


Figure 8. The influence of hole and electron doping on the I_{2D}/I_G .⁸⁰

graphene layers,⁸¹ and I_G/I_{2D} was related to the thickness of the graphene.^{82,83} Thus, for N-graphene with inhomogeneous layers, the I_{2D}/I_G cannot reflect the nitrogen doping level.³⁹⁰ I_{2D}/I_G can be used only when N-graphene has homogeneous layers.³⁹¹

Before using I_D/I_G and I_{2D}/I_G to characterize N-graphene, inhomogeneous nitrogen doping should be considered. It has been reported that some spots showed high I_D/I_G and some showed very low I_D/I_G within the N-graphene,⁴⁰ which suggests the nonuniform defect distribution induced by inhomogeneous nitrogen incorporation. Thus, the I_D/I_G and I_{2D}/I_G derived from the Raman spectra at discrete spots cannot fully reflect the doping situation. In practice, Raman spectral mapping can be used to avoid this problem. This technique records the Raman spectra on a large scale; thus, the comparison of different N-graphenes is more convincing for inhomogeneous doping. In the maps of I_{2D}/I_G over a $80 \times 80 \mu\text{m}^2$ area (Figure 9b),⁸⁴ the pristine graphene shows a higher I_{2D}/I_G , which means a lower carrier concentration. The more area of low I_{2D}/I_G in N-graphene grown under higher NH_3 ratio corresponds to a higher carrier concentration. Moreover, it is observed that the size of the purple paths depends on the doping level, which

indicates the purple paths are related to the local dopant concentration.⁴⁰⁹
410

Some studies reported a shift of the G band after nitrogen doping. Because the variation of charge density in pristine graphene will cause the different G band positions and I_{2D}/I_G in the different spots of graphene,⁸⁵ Li et al. made a gold marker in the vicinity of graphene to accurately monitor the evolution of the nitrogen doping.⁷⁰ An upshift of the G band in the Raman spectra of the monolayer graphene was observed. In the work of Zhao et al.,⁸⁴ a similar trend of the G band was also observed by using the frequency histogram collected from Raman spectral mapping (Figure 9d). However, the observed position of the G band can also be affected by the inhomogeneous layer distribution^{82,86} and defects due to nitrogen doping,⁸⁷ which may induce the downshift of G band in N-graphene in some studies.^{52,63} Thus, comprehensive consideration should be taken if discussing this phenomenon.⁴²⁴
425

3.3. Scanning Tunneling Microscopy (STM). STM is a very powerful technique to investigate the electronic properties of a sample. It can probe the charge density at the Fermi level. When the bias voltage (V_{bias}) applied between the tip and sample is positive, electrons tunnel from the tip into the specimen, then the lowest unoccupied states of the specimen are probed. When a negative V_{bias} is applied, electrons tunnel from the specimen into the tip, and the highest occupied states of specimen are probed.⁸⁸ Due to the sharp tip, the STM images can show atomic resolution. Recently, both theoretical and experimental studies on the electronic properties of N-graphene have been carried out.^{52,84,89}
437

Compared with the pristine graphene, N-graphene shows some brighter sections that are distinct from the main graphene network in the STM image (Figure 10c).^{52,84} Different bright features correspond to different nitrogen doping types. Because these bright sections are only a few atoms across (<1 nm), they cannot be defects induced by nitrogen doping.⁵² Through the STM line scan over the bright section and graphene lattice (Figure 10a), an out-of-plane height of $0.6 \pm 0.2 \text{ \AA}$ is observed. This indicates the substitution of nitrogen atoms in graphene. The calculated STM image shows that the C atoms neighboring

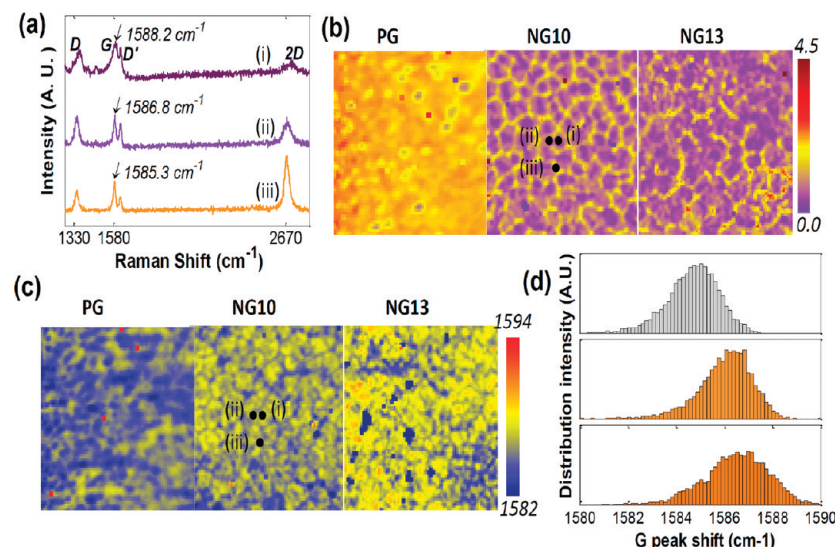


Figure 9. (a) Raman spectra taken at different positions over N-graphene grown under 0.1 Torr NH_3 (NG10). (b) Maps of I_{2D}/I_G for pristine graphene, NG10, and N-graphene grown under 0.13 Torr NH_3 (NG13). (c) Maps of the G band frequency for PG, NG10, and NG13 samples. (d) G band frequency histogram of PG, NG10, and NG13 from the maps in part c.⁸⁴

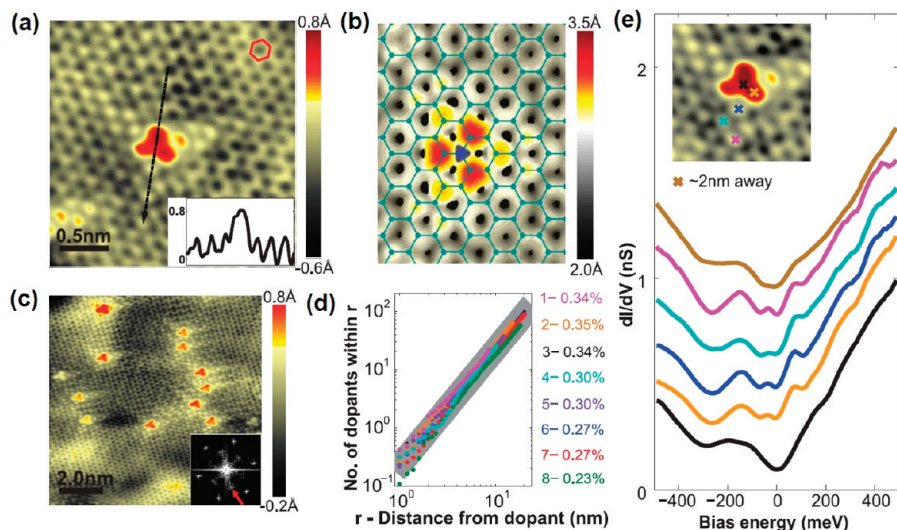


Figure 10. (a) STM image of the most common doping form in N-graphene. The inset is the line profile across the dopant ($V_{\text{bias}} = 0.8$ V, $I_{\text{set}} = 0.8$ nA). (b) Simulated STM image of quaternary N dopant based on density functional theory calculations ($V_{\text{bias}} = 0.5$ V). (c) STM image of N-graphene showing ~ 14 quaternary N dopants. The inset is the FFT of topography ($V_{\text{bias}} = 0.8$ V, $I_{\text{set}} = 0.8$ nA). (d) Spatial distribution of N–N distances from eight samples with different nitrogen concentrations. (e) dI/dV curves taken from an N atom and other nearby bright topographic features ($V_{\text{bias}} = 0.8$ V, $I_{\text{set}} = 1.0$ nA).⁸⁴

448 N atoms exhibit the brightest feature because of the increased
449 charge density of state induced by the neighbor N atoms
450 (Figure 10b).^{52,84}

451 Apart from the local structure around dopants, some long
452 “tails” arising from the intervalley electron scattering are
453 observed in the STM image (Figure 10c). This kind of
454 scattering is verified by the inner hexagon in the fast Fourier
455 transform (FFT). STM is also used to study the possibility of
456 dopant clustering. The dopant distribution in the N–N
457 distance is quadratic even when the distance is down to few
458 lattice constants (Figure 10d); it indicates that the dopants
459 distribute randomly. Furthermore, the same study reveals that
460 nearby dopants prefer to substitute into the same sublattice of
461 graphene. The charge-carrier density of N-graphene can be
462 measured from a STM study. From the curves of dI/dV
463 (derivative of current with respect to the voltage), the Dirac
464 point of N-graphene is calculated (Figure 10e). Then the
465 charge-carrier density can be calculated from the relation $n =$
466 $E_D^2/\pi(\hbar\nu_F)^2$ (n is the charge-carrier density, \hbar is the Plank’s
467 constant over 2π , ν_F is the Fermi velocity).

468 **3.4. Other Characterization Techniques.** In addition to
469 the above techniques, scanning electron microscope (SEM),
470 HRTEM, atomic force microscope (AFM), selected area
471 electron diffraction (SAED) and thermogravimetric analysis
472 (TGA) have also been used to study N-graphene. Specifically,
473 SEM is commonly employed to study the morphology of N-
474 graphene. HRTEM is the most commonly used technique to
475 determine the number of graphene layers on the basis of the
476 cross section or edge images of N-graphene. AFM can also be
477 used to estimate the number of graphene layers on the basis of
478 the interlayer distance. SAED can provide information about
479 the crystalline structure of N-graphene on the basis of
480 diffraction pattern. The hexagonal diffraction spots indicate
481 that the N-graphene still keeps a well-ordered crystalline
482 structure,^{44,62} and the ringlike diffraction pattern of spots
483 means structure distortion occurs after doping.⁴¹

4. APPLICATIONS

484 **4.1. Electrocatalyst for Fuel Cell Application.** A fuel cell
485 is an electrochemical energy conversion device that oxidizes
486 fuel at the anode and reduces oxygen from air at the cathode to
487 produce electricity.⁹⁰ Commonly, Pt is used as the catalyst for
488 the oxidation reaction on the anode and reduction reaction on
489 the cathode. However, the commercial application of Pt catalysts is
490 limited by its scarcity, time-dependent drift, and CO poison-
491 ing.⁹⁰ Thus, Pt-based catalysts^{91,92} and other metal catalysts,⁹³ such as Au and Pd,^{93,94} have been developed. Recently, N-
492 graphene has been used in fuel cells as either the catalysts
493 directly or carbon support to anchor metal catalysts.⁴⁹⁴

495 **4.1.1. Theoretical Part.** The oxygen reduction reaction of N-
496 graphene on the cathode of a fuel cell has been discussed in
497 many studies. Through studying the ORR behavior of model
498 graphenes $C_{45}NH_20$ and $C_{45}NH_18$ in acidic environment, Zhang
499 et al.²⁵ showed that the spin density and charge density of
500 atoms were the major factors that determined the catalytic
501 active sites in ORR. The substitution of N atoms, which
502 introduces the unpaired electron, will change the atomic charge
503 distribution. The active sites in N-graphene usually are carbon
504 atoms that possess high spin density. If the spin density is
505 negative and small, the atom with a higher charge density will
506 be the active sites. Although in a previous study,⁹⁵ it was shown
507 that the energy gap between highest occupied molecular orbital
508 (HOMO) and lowest unoccupied molecular orbital (LUMO)
509 could be used as an index of kinetic stability, it is unnecessarily
510 related to the catalytic capacity of graphene and N-graphene.⁵¹⁰

511 The ORR mechanism on N-graphene also has been studied.⁵¹¹
512 Earlier studies have shown that O_2 could be reduced following
513 two pathways. One is a direct four-electron pathway in which
514 O_2 is reduced to water in an acidic environment or OH^- in an
515 alkaline environment. Another is a two-electron pathway in
516 which O_2 is partly reduced to H_2O_2 in an acidic environment or
517 OOH^- in an alkaline environment. Both mechanisms have
518 been proposed by theoretical studies based on different N-
519 graphene models. Kurak et al.⁹⁶ showed a two-electron ORR
520 pathway based on the graphene model possessing two neighbor
520

s21 N atoms in the zigzag edge. However, it was found that two s22 nitrogen atoms were very unlikely to be doped at two s23 neighboring zigzag sites by checking the interaction energy s24 between two nitrogen atoms.⁹⁷

Zhang et al.²⁵ proposed a four-electron ORR pathway on N-graphene in an acidic environment. Furthermore, after taking the solvent, surface coverage, and adsorbates into consideration, Yu et al.⁹⁸ obtained the overall energy profile of the ORR pathway on N-graphene in an alkaline environment. The study shows that water molecules are essential for the reaction. The O_2 adsorption is greatly enhanced due to the O_2 polarization induced by the hydrogen bonding with water. Through investigating two ORR mechanisms, dissociative and associative (Figure 11), study shows that the associative mechanism is

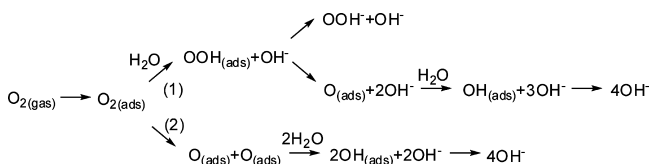


Figure 11. Scheme of the ORR reaction on N-graphene in an alkaline environment where 1 is the associative mechanism and 2 is the dissociative mechanism.⁹⁸

more energetically favored in ORR because of the lower O_2 dissociation barrier. In the associative mechanism, the desorption barrier of $OOH_{(ads)}$ into OOH^- is high, so the energetically favored reaction $OOH_{(ads)} \rightarrow O_{(ads)} + OH^-$ is more likely to happen, which suggests the four-electron ORR pathway of N-graphene. The reaction rate is determined by the removal of $O_{(ads)}$ on the surface of N-graphene.

Apart from N-graphene, the interaction between Pt atom and N-graphene has been investigated.²⁶ In N-graphene, the nitrogen atoms do not bond with Pt atom directly; instead, they direct a Pt atom to bond with the carbon atom, which is more energetically favored. This is helpful to prevent Pt nanoclusters from migrating and forming larger particles. Because the introduction of nitrogen atoms disrupts the delocalized double bond in the graphene system, the Pt/C bond will focus on the 6s/2s orbitals rather than 5d/2p orbitals. This doubles the binding energy between Pt and carbon atoms. In general, the binding of Pt to N-graphene improves the catalytic durability of Pt.

4.1.2. Experimental Part. Several groups have recently reported studies on metal-free N-graphene with enhanced catalytic activity toward ORR.^{23,40,41,52,60,62} The efficiency of ORR can be evaluated through two ways.⁹⁹ One way is to calculate the transfer number of electrons through the Koutecky–Levich (K–L) equation by using a rotating disk electrode (RDE). Another way is to measure the proportion of H_2O_2 formed during the ORR process by using a rotating ring-disk electrode. Qu et al.⁴¹ reported that N-graphene exhibited a typical one-step, four-electron ORR pathway, which is similar to the ORR pathway of a Pt catalyst (Figure 12a). In contrast, pristine graphene showed a two-step, two-electron ORR pathway with a lower onset potential. In another work,⁶⁰ the H_2O_2 formed in the ORR process was about 10% at -0.5 V in the diffusion-controlled region. The low proportion of H_2O_2 indicated the four electron reduction process dominated in ORR. All these studies show that N-graphene can be a very effective catalyst for ORR.

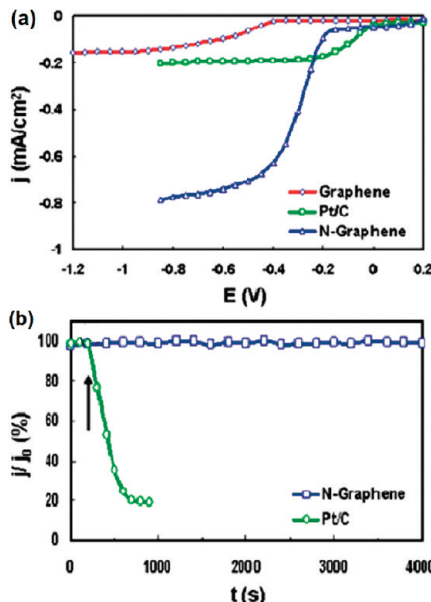


Figure 12. (a) RRDE voltammograms for ORR in air-saturated 0.1 M KOH on the electrodes graphene (red), Pt/C (green), and N-graphene (blue) with a scan rate of 0.01 V s^{-1} . Electrode rotating rate: 1000 rpm. (b) Current–time chronoamperometric response of Pt/C and NG to CO. The arrow indicates the addition of 10% (v/v) CO at -0.4 V.⁴¹

Furthermore, the ORR activity of N-graphene is also studied through diffusion limited current and kinetic current. Some studies showed the diffusion-limited current density of N-graphene was higher than commercial 20% or 40% Pt/C (E-TEK) catalyst,^{41,52} but another study showed that N-graphene had a similar diffusion-limited current density.⁶⁰ Although the reported activity of N-graphene varies from different studies,⁵⁷⁸ there is consensus that N-graphene has excellent stability compared with the Pt catalyst. Shao et al.²³ reported that the 20% Pt/C (E-TEK) showed higher electrocatalytic activity than N-graphene before an accelerated degradation test (ADT), but after the ADT, the N-graphene exhibited higher kinetic current compared with the Pt/C catalyst because of the degradation of Pt/C. In addition, studies also showed the activity of N-graphene would not be influenced by the addition of methanol or CO (Figure 12b).^{23,41} These two advantages make N-graphene a promising material toward ORR in fuel cells.

Notably, in the above studies in which the four-electron ORR pathway was observed, these N-graphene catalysts consist of two or three nitrogen types.^{23,41,52,60,62} For N-graphene possessing only the pyridinic N, a two-electron reduction process was observed in the ORR process.⁴⁰ This may indicate a less efficient ORR performance of pyridinic N. In another study, the N-graphene with higher pyridinic and quaternary N content exhibited a higher onset potential than N-graphene that possessed the same nitrogen content. This suggests the pyridinic and quaternary N may play a more important role for ORR activity.⁶⁰ However, because of the scarcity of study in this field and variation in experimental conditions, the relationship between the catalytic activity and the nitrogen species is still unclear. In the former study of N-CNTs, both quaternary^{100,101} and pyridinic^{21,24} nitrogen have been observed to have the dominant effect for the ORR activity. Thus, further research work on the nitrogen catalytic site is still required.

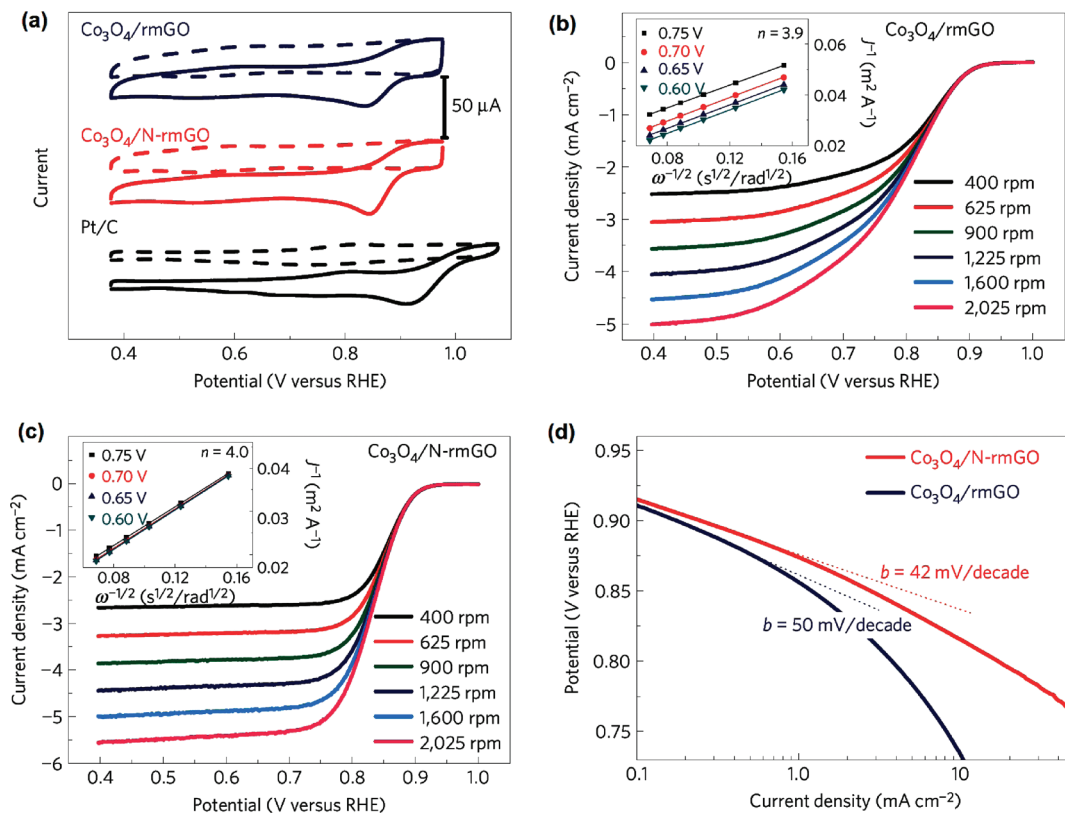


Figure 13. (a) Cyclic voltammetry (CV) of $\text{Co}_3\text{O}_4/\text{rmGO}$, $\text{Co}_3\text{O}_4/\text{N-rmGO}$ and Pt/C in O_2^- (solid line) or Ar-saturated (dashed line) 0.1 M KOH solution. RDE voltammograms of $\text{Co}_3\text{O}_4/\text{rmGO}$ (b) and $\text{Co}_3\text{O}_4/\text{N-rmGO}$ (c) for ORR in O_2 -saturated 0.1 M KOH at different rotation rates with a scan rate of 5 mV s^{-1} . The inset figure is the corresponding Koutecky–Levich plots at different potentials.¹⁰⁴

Apart from the nitrogen types, the nitrogen content is also related to the ORR activity of N-graphene. However, because N-graphene usually consists of two or three nitrogen types and the content of different nitrogen types usually varies with different nitrogen doping levels, different studies have produced contradictory results in previous studies.^{52,62} In a more direct study in which N-graphene contains only pyridinic N,⁴⁰ the N-graphene possessing the higher nitrogen content (16 at. %) exhibited poorer ORR activity than that possessing the lower nitrogen content (2.2 at. %). In a theoretical study, it has been reported that model graphene with a higher nitrogen content was more easily poisoned by $\text{O}_{(\text{ads})}$ because of the stronger affinity.¹⁰² These results mean an optimal nitrogen content might be critical to achieving a high ORR activity.

Several studies also have studied the performance of Pt/N-graphene in both oxidation and reduction reactions.^{67,73} For Pt/N-graphene used for an oxidation reaction,⁷³ it has been reported that Pt nanoparticles could disperse better on the surface of N-graphene with the existence of N atoms in a carbon lattice. Moreover, the conductivity of N-graphene was improved at high temperature (800 °C). These two factors made Pt/N-graphene exhibit a 3 times higher oxidation current than 20% Pt/graphene black catalyst. For Pt/N-graphene used for the oxygen reduction reaction,⁶⁷ it also showed an improved performance compared with Pt/graphene because of the better dispersion of Pt nanoparticles and stronger interaction between Pt and C atoms stated in the theoretical part.²⁶

Apart from the Pt catalyst, other nonprecious metal catalysts supported on N-graphene toward ORR have been studied.^{103,104} Tsai et al.¹⁰³ synthesized FeCN/N-graphene by

impregnating N-graphene into a mixture of iron acetate and 1,10-phenanthroline, then the Fe_xC species formed in the sintering process would anchor the FeCN nanoparticles on N-graphene surface. The as-synthesized FeCN/N-graphene shows an enhanced ORR activity compared with the N-graphene because of the additional ORR activity of FeCN nanoparticles.⁶⁴² In another notable study,¹⁰⁴ Liang et al. grew Co_3O_4 on mildly oxidized graphene oxide (rmGO) with or without the presence of NH_4OH , then catalyst $\text{Co}_3\text{O}_4/\text{rmGO}$ and $\text{Co}_3\text{O}_4/\text{N-rmGO}$ were obtained. The latter catalyst has ~4 at. % nitrogen content. Through the ORR study of the $\text{Co}_3\text{O}_4/\text{rmGO}$ and $\text{Co}_3\text{O}_4/\text{N-rmGO}$, it has been revealed that these two catalysts exhibit high ORR activity that is different from the Co_3O_4 nanocrystals (Figure 13a). Also different from the two-electron ORR pathway of N-rmGO obtained in the study, these two catalysts show the obvious four-electron ORR pathway (Figure 13b, c). Comparing the kinetic current of $\text{Co}_3\text{O}_4/\text{N-rmGO}$ with $\text{Co}_3\text{O}_4/\text{rmGO}$, the former exhibits the apparent higher current density than the latter (Figure 13d). The higher ORR activity of $\text{Co}_3\text{O}_4/\text{N-rmGO}$ is ascribed to the synergistic coupling between Co_3O_4 and N-graphene. Because $\text{Co}_3\text{O}_4/\text{N-rmGO}$ shows both the high ORR activity similar to Pt catalyst and excellent stability, this kind of hybrid catalyst is also promising for ORR catalysis.

4.2. Field-Effect Transistor (FET). For semiconductors, the flow of electricity needs some kind of activation (for example, heat or light absorption) to get over the gap between the valence band and conduction band.¹⁰⁵ If the semiconductor is activated by the external electric field to switch “on” and “off”, then it is called FET. Generally speaking, the large-scale

and bilayer graphene do not possess a band gap; however, constraining large-scale graphene in one dimension (GNRs) or applying an electric field perpendicularly on the bilayer graphene can induce the band gap (Figure 14).¹⁰⁶ Recently, both theoretical and experimental works have studied the semiconductor properties of N-graphene.

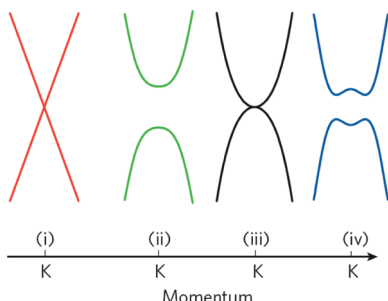


Figure 14. Band structure around the k point of (i) large-area graphene, (ii) graphene nanoribbons, (iii) unbiased bilayer graphene, and (iv) bilayer graphene with an applied perpendicular field.¹⁰⁶

4.2.1. Theoretical Part. Nitrogen doping can effectively modulate the electrical properties of graphene. On the basis of the investigation of C_3N_4 and $C_6N_9H_3$ graphene,²⁹ it has been revealed that the band gap of N-graphene with a high N/C ratio reached ~ 5 eV. The band gap can be tuned by the presence of external stress or adatoms. In another theoretical work based on the study of delta-doping graphene,¹⁰⁷ it has been reported that the band gap could be opened only when the nitrogen content was over $\sim 25\%$. However, delta-doping may be unlikely to occur in practice. In the experimental study, an obvious band gap has been observed on N-graphene with a lower nitrogen content.⁷⁰ Apart from the band gap, the mobility and conductivity of N-graphene has also been discussed theoretically by using the quantum-mechanical

Kubo-Greenwood approach.²⁷ When the nitrogen concentration (C_d) is over or equal to 2% ($2\% \leq C_d \leq 4\%$), the decay of the diffusion coefficient D is clearly observed. This indicates the onset of quantum interference effects. However, this effect is still weak and can only marginally affect the conduction when the nitrogen content is low. This study suggests that the nitrogen doping may modulate the graphene property while maintaining good mobility and conductivity. However, the conduction is also influenced by many other factors. In experimental study, it has been shown that both defects and nitrogen atoms will be introduced into graphene. Defects can serve as the scattering center, which will affect the mobility of N-graphene. Moreover, when the nitrogen concentration rises over 5%, a stronger localization effect might occur, which will largely decrease the mobility in N-graphene.²⁷

GNR can be obtained by constraining large-scale graphene to one dimension. Former studies have revealed that H-terminated GNRs with either armchair or zigzag-shaped edges have nonzero band gaps.^{79,108} Through theoretical studies of zigzag GNR (ZGNR),^{109,110} it was revealed that the nitrogen atom and defects energetically preferred to dope at the edge of GNR. Depending on doping sites and various GNRs, the introduction of nitrogen atoms will induce very different electronic properties. For example, Yu et al.¹⁰⁹ showed different nitrogen doping sites would make the impurity state lie below or above the Fermi level. Li et al.¹¹⁰ found one edge-doped nitrogen made ZGNR spin a gapless semiconductor while two opposite edge-doped nitrogens made ZGNR nonmagnetic metals. Biel et al.¹¹¹ reported that the full suppression of impurity backscattering would occur if the doped GNR was armchair and mirror-symmetrical.

4.2.2. Experimental Part. After the preparation of bottom-gated N-graphene FET by using a Si substrate with a 500 nm thick SiO_2 layer (Figure 15a), pristine graphene exhibits p-type behavior because of the adsorption of oxygen or water in air (Figure 15b). In contrast, N-graphene with an 8.9 at. % nitrogen

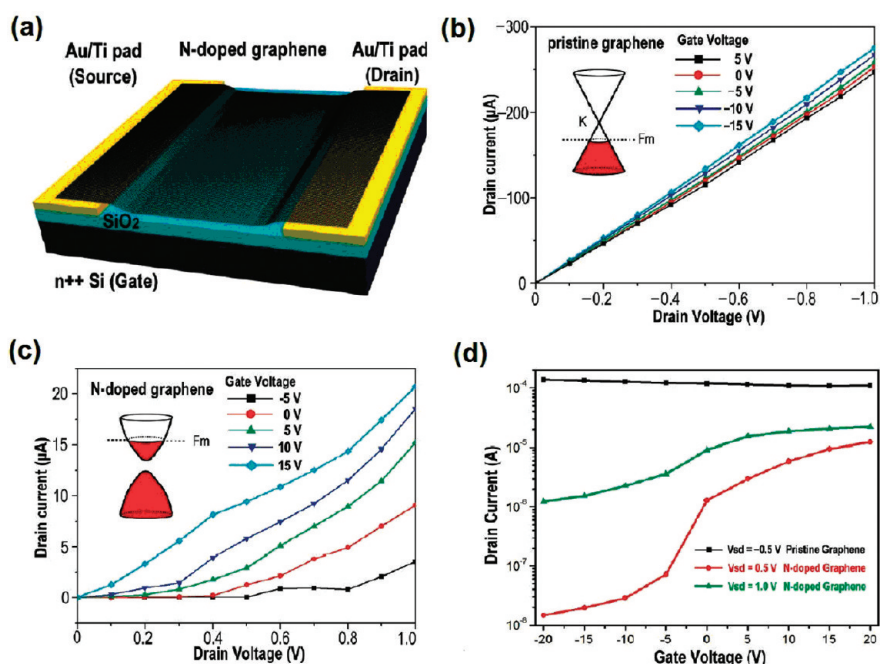


Figure 15. (a) Schematic illustration of the N-graphene FET device. (b, c) I_{ds}/V_{ds} characteristics at various V_g 's for the pristine graphene and NG FET device. (d) Transfer characteristics of the pristine graphene and NG.³⁰

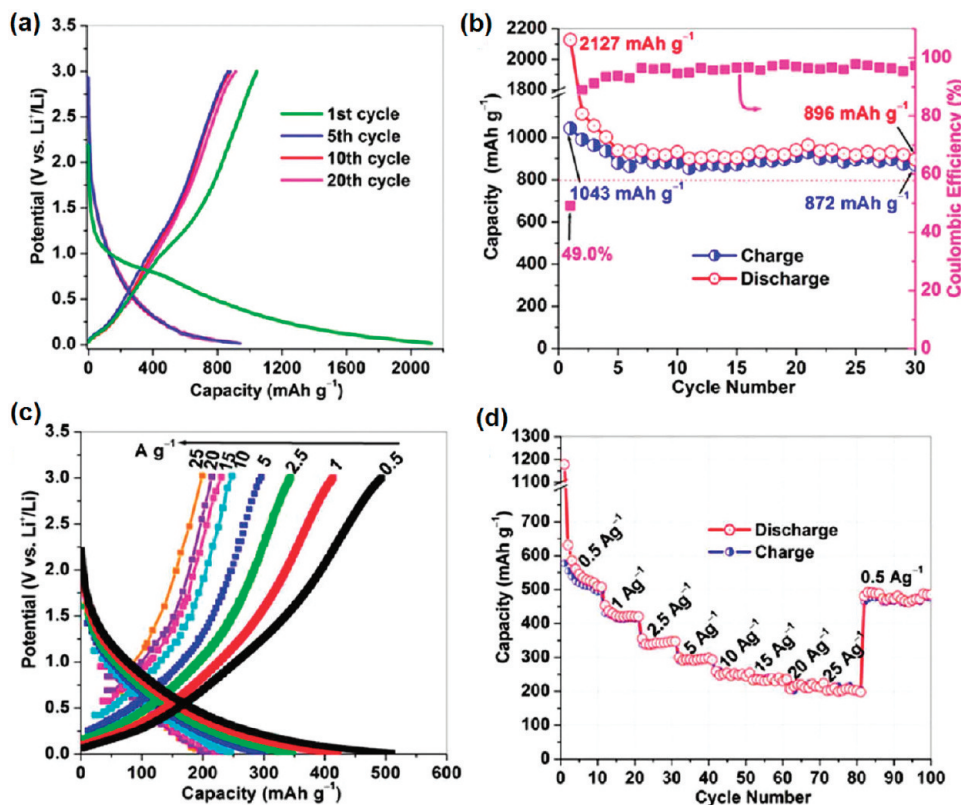


Figure 16. Galvanostatic charge–discharge profile of N-graphene at a low current rate of 50 mA/g (a) and a higher current rate from 0.5 to 25 A/g (c), (b) cycle performance and Coulombic efficiency of N-graphene at low current rate of 50 mA/g, (d) cycle performance and rate capabilities of N-graphene at higher current rate from 0.5 to 25 A/g.¹¹⁵

doping level exhibits typical n-type semiconductor behavior (Figure 15c, d).³⁰ Compared with the mobility of pristine graphene ($300\text{--}1200\text{ cm}^2\text{ V}^{-1}\text{ s}^{-1}$), the mobility of N-graphene reduces to $200\text{--}450\text{ cm}^2\text{ V}^{-1}\text{ s}^{-1}$. Using different precursors in the CVD method, Jin et al.⁴⁴ reported the mobility of N-graphene with 2.4 at. % nitrogen content reduced by 2 orders of magnitude compared with that of pristine graphene. In other methods,^{50,59,63} such as N-graphene obtained through NH₃ annealing after N⁺ ion irradiation,⁵⁹ a much lower hole and electron conductivity was observed compared with the pristine graphene.

In the study of nitrogen-doped GNR (N-GNR), it has been reported the N-GNR fabricated by high power electrical annealing in NH₃ showed typical n-type semiconductor behavior, and the mobility was similar with the GNR annealed in vacuum.³¹ The reason is that nitrogen atoms incorporate mainly into the edge of GNR, and few charged impurities are introduced, which will not degrade the mobility of GNR.

As discussed above, the electron mobility of graphene decreases with the increment of band gap in most cases, which is similar to the trend in studies of CNTs.^{106,112,113} Although several theoretical studies^{27,111} and the recent work about N-GNR³¹ have shown the mobility of N-graphene might be maintained by controlling the nitrogen at a low doping level and specific doping site, the scattering center induced by the defects will drastically decrease the mobility of N-graphene in practice. In addition, it is claimed that the grain boundaries in N-graphene may also contribute to a decrement of mobility.³⁶ Other than the mobility, a sizable band gap, preferably 0.4 eV or higher, is also required in conventional FET (the band gap of silicon is 1.1 eV).¹⁰⁶ Until now, only a few studies of N-

graphene have reported a band gap in their works. Zhang et al.⁷⁵⁴ showed the band gap in N-graphene with 2.9 at. % nitrogen⁷⁵⁵ content was about 0.16 eV,⁵⁰ which is still too low. Considering⁷⁵⁶ the mobility and band gap of N-graphene obtained up to the⁷⁵⁷ present, synthesis of N-graphene for practical applications⁷⁵⁸ is still far off.⁷⁵⁹

4.3. Lithium Ion Batteries. In recently years, graphene has attracted great attention as a potential anode material in lithium ion batteries (LIBs) because of its fascinating properties, such as high electrical electronic properties, high surface area, and excellent mechanical flexibility. Although graphene-based materials can reach a high reversible capacity (1013–1054 mA h/g) at a low charge rate,¹¹⁴ it is still rate-limited at a high charge/discharge rate (≥ 500 mA/g).¹¹⁵ Thus, a N-graphene-based device is proposed with the intent to achieve a high reversible capacity at the high charge/discharge rate.

In earlier work, Reddy et al.⁴³ obtained N-doped graphene under the control of a CVD method. The reversible discharge capacity of N-graphene was almost double compared with pristine graphene because of the enhanced Li ion intercalation with the introduction of nitrogen atoms. In another more recent work,¹¹⁶ N-GNS with 2 at. % nitrogen content (57.4% pyridinic, 35.0% pyrrolic, and 7.6% quaternary N) was synthesized by heat treatment of GO in an NH₃ atmosphere. The N-graphene possessed a reversible capacity of around 900 mA h/g at a current density of 42 mA/g and a capacity of ~ 250 mA h g⁻¹ at a high current density of 2.1 A/g. In another work in which N-graphene was synthesized by a similar heat treatment method,¹¹⁵ N-graphene with 3.13 at. % nitrogen content exhibited reversible capacities of 1043 mAh/g and 872 mAh/g in the first and 31st cycles at a low current rate of 50 mA/g.

f16

785 mA/g, respectively (Figure 16 a, b). At a higher current rate of
 786 25 A/g, the reversible capacities of N-graphene still reached 199
 787 mAh/g (Figure 16 c, d).

788 The excellent performance of N-graphene can be ascribed to
 789 many factors, such as the introduction of nitrogen atoms, the
 790 defects and disordered surface morphology induced by doping,
 791 increased electrode/electrolyte wettability, and improved
 792 electrochemical performance. Notably, in the above studies,
 793 the types of pyridinic and pyrrolic N are predominant in the N-
 794 graphene. Through the study of nitrogen-doped graphite, it has
 795 been revealed that both the pyridinic and quaternary N played
 796 an effective role in lithium intercalation and extraction.¹¹⁷ Thus,
 797 graphene with a large quaternary N content might also be used
 798 in LIBs.

799 **4.4. Devices in Other Fields.** N-Graphene has been
 800 applied in the field of ultracapacitors.⁶⁹ The ultracapacitor
 801 based on N-graphene has shown a long cycle life (Figure 17a).

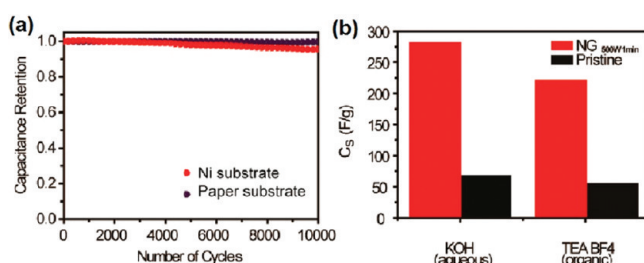


Figure 17. (a) The cycling tests for the ultracapacitors based on Ni and paper substrates up to 10 000 cycles. (b) The specific capacitances measured in 6 M KOH and organic electrolytes.⁶⁹

802 Moreover, a N-graphene-based device showed a much higher
 803 capacitance than a device based on pristine graphene in both
 804 KOH and organic electrolyte (Figure 17b). By calculating the
 805 binding energy between the potassium ion and nitrogen
 806 configurations at different positions of N-graphene, it has been
 807 revealed that the basal-plane pyridinic N exhibited the largest
 808 binding energy. Thus, basal-plane pyridinic N was claimed to
 809 have a dominant role in the capacitance enhancement. Pyrrolic
 810 N also showed a large binding energy with ion, but the negative
 811 charge of pyrrolic N would cause too strong binding for the
 812 reversible charging/discharging process, which was reflected by
 813 the lower Coulombic efficiencies of N-graphene with a large
 814 proportion of pyrrolic N. Therefore, controlling the appropriate
 815 nitrogen configuration can greatly promote the capacitance of
 816 N-graphene.

817 Study has shown that N-graphene has a better electron
 818 transfer efficiency than pristine graphene,^{68,72} rendering its
 819 potential use for electrochemical sensing. Because GO_x could
 820 oxidize glucose with oxygen and produce gluconic acid and
 821 H₂O₂, in the study of Wang et al.,⁶⁸ the glucose sensor was
 822 fabricated by immobilizing glucose oxidase (GO_x) on the
 823 biocompatible N-graphene surface. It was observed that the
 824 GO_x redox peak current on N-doped graphene was greatly
 825 improved over that on graphene, which demonstrated the
 826 enhanced electron transfer efficiency of N-graphene. This kind
 827 of biosensor shows a good response for glucose concentrations
 828 ranging from 0.01 to 0.5 mM in the presence of other
 829 molecules.

830 Apart from the above applications, N-graphene also has been
 831 used as a support to anchor quantum dots toward high-
 832 performance photocatalysts.¹¹⁸ N-Graphene/CdS nanocompo-

sites have a higher photocatalytic activity than graphene/CdS⁸³³
 and pure CdS, which can be attributed to the hampering of the⁸³⁴
 radiative recombination of the electron–hole pairs, which is⁸³⁵
 induced by enhanced electron transportation from CdS to N-⁸³⁶
 graphene. Moreover, CdS anchored on N-graphene with 2 wt⁸³⁷
 % nitrogen content showed the best catalytic activity. It reveals⁸³⁸
 that a proper junction structure is required for the highest⁸³⁹
 photocatalytic activity.⁸⁴⁰

5. CONCLUSION

In summary, many research works on N-graphene have⁸⁴¹
 emerged in recent years. Various synthesis approaches and⁸⁴²
 characterization techniques have been explored to obtain and⁸⁴³
 characterize N-graphene. The N doping offers an effective way⁸⁴⁴
 to tailor the properties of graphene, thus making N-graphene a⁸⁴⁵
 promising material for use in many fields. However, the method⁸⁴⁶
 for the production of large-scale N-graphene is still lacking;⁸⁴⁷
 thus, new methods are required. Moreover, synthesizing N-⁸⁴⁸
 graphene meets problems similar to those encountered during⁸⁴⁹
 fabricating N-CNT. First, controlling the nitrogen type and⁸⁵⁰
 distribution is unresolved. Second, to achieve nitrogen doping⁸⁵¹
 at specific positions and with precise control of doping content⁸⁵²
 is still a challenge. For FET application, the doping location and⁸⁵³
 doping content is critical not to decrease the electron mobility⁸⁵⁴
 drastically while opening a suitable band gap. For electro-⁸⁵⁵
 catalysis, the correlation between the activity and nitrogen type⁸⁵⁶
 needs to be identified, and controlling the specific nitrogen type⁸⁵⁷
 in N-graphene is required for high performance catalysts. For⁸⁵⁸
 other applications, such as LIBs and ultracapacitors, a specific⁸⁵⁹
 nitrogen type may also be required. Another issue to be⁸⁶⁰
 considered is defects and distortion. Defects are inevitable⁸⁶¹
 during the synthesis process of N-graphene. Defects will⁸⁶²
 decrease the mobility of N-graphene; however, their presence⁸⁶³
 will benefit the catalytic reaction for ORR and LIBs. Depending⁸⁶⁴
 on the application, choosing or finding an appropriate approach⁸⁶⁵
 is required.⁸⁶⁶

■ AUTHOR INFORMATION

Corresponding Author

*Phone: (65) 6316 8866. Fax: (65) 6794 7553. E-mail: WangXin@ntu.edu.sg.

Notes

The authors declare no competing financial interest.

■ ACKNOWLEDGMENTS

This work is supported by the academic research fund AcRF⁸⁷⁴
 tier 2 (MOE2009-T2-2-024), Ministry of Education, Singapore,⁸⁷⁵
 and competitive research program (2009 NRF-CRP 001-032),⁸⁷⁶
 National Research Foundation, Singapore.⁸⁷⁷

■ REFERENCES

- (1) Novoselov, K. S.; Geim, A. K.; Morozov, S. V.; Jiang, D.; Zhang, Y.; Dubonos, S. V.; Grigorieva, I. V.; Firsov, A. A. *Science* **2004**, *306*, 666.
- (2) Stoller, M. D.; Park, S.; Zhu, Y.; An, J.; Ruoff, R. S. *Nano Lett.* **2008**, *8*, 3498.
- (3) Balandin, A. A.; Ghosh, S.; Bao, W.; Calizo, I.; Teweldebrhan, D.; Miao, F.; Lau, C. N. *Nano Lett.* **2008**, *8*, 902.
- (4) Lee, C.; Wei, X.; Kysar, J. W.; Hone, J. *Science* **2008**, *321*, 385.
- (5) Barone, V.; Hod, O.; Scuseria, G. E. *Nano Lett.* **2006**, *6*, 2748.
- (6) Kosynkin, D. V.; Higginbotham, A. L.; Sinitskii, A.; Lomeda, J. R.; Dimiev, A.; Price, B. K.; Tour, J. M. *Nature* **2009**, *458*, 872.

- 890 (7) Li, X.; Wang, X.; Zhang, L.; Lee, S.; Dai, H. *Science* **2008**, *319*,
891 1229.
- 892 (8) Ponomarenko, L. A.; Schedin, F.; Katsnelson, M. I.; Yang, R.;
893 Hill, E. W.; Novoselov, K. S.; Geim, A. K. *Science* **2008**, *320*, 356.
- 894 (9) Ritter, K. A.; Lyding, J. W. *Nat. Mater.* **2009**, *8*, 235.
- 895 (10) Jiao, L.; Zhang, L.; Wang, X.; Diankov, G.; Dai, H. *Nature* **2009**,
896 *458*, 877.
- 897 (11) Derycke, V.; Martel, R.; Appenzeller, J.; Avouris, P. *Appl. Phys.*
898 *Lett.* **2002**, *80*, 2773.
- 899 (12) Gong, K.; Du, F.; Xia, Z.; Durstock, M.; Dai, L. *Science* **2009**,
900 *323*, 760.
- 901 (13) Wang, S. Y.; Wang, X.; Jiang, S. P. *Langmuir* **2008**, *24*, 10505.
- 902 (14) Wang, S. Y.; Yang, F.; Chen, S. L.; Jiang, S. P.; Wang, X. *Electrochim. Commun.* **2010**, *12*, 1646.
- 903 (15) Zhou, C.; Kong, J.; Yenilmez, E.; Dai, H. *Science* **2000**, *290*,
904 1552.
- 905 (16) Schedin, F.; Geim, A. K.; Morozov, S. V.; Hill, E. W.; Blake, P.;
906 Katsnelson, M. I.; Novoselov, K. S. *Nat. Mater.* **2007**, *6*, 652.
- 907 (17) Giovannetti, G.; Khomyakov, P. A.; Brocks, G.; Karpan, V. M.;
908 van den Brink, J.; Kelly, P. J. *Phys. Rev. Lett.* **2008**, *101*, 026803.
- 909 (18) Chen, W.; Chen, S.; Qi, D. C.; Gao, X. Y.; Wee, A. T. S. *J. Am.*
910 *Chem. Soc.* **2007**, *129*, 10418.
- 911 (19) Ewels, C. P.; Glerup, M. *J. Nanosci. Nanotechnol.* **2005**, *5*, 1345.
- 912 (20) Casanovas, J.; Ricart, J. M.; Rubio, J.; Illas, F.; Jiménez-Mateos, J.
913 M. *J. Am. Chem. Soc.* **1996**, *118*, 8071.
- 914 (21) Kundu, S.; Nagaiah, T. C.; Xia, W.; Wang, Y.; Dommele, S. V.;
915 Bitter, J. H.; Santa, M.; Grundmeier, G.; Bron, M.; Schuhmann, W.;
916 Muhler, M. *J. Phys. Chem. C* **2009**, *113*, 14302.
- 917 (22) Matter, P. H.; Zhang, L.; Ozkan, U. S. *J. Catal.* **2006**, *239*, 83.
- 918 (23) Shao, Y.; Zhang, S.; Engelhard, M. H.; Li, G.; Shao, G.; Wang,
919 Y.; Liu, J.; Aksay, I. A.; Lin, Y. *J. Mater. Chem.* **2010**, *20*, 7491.
- 920 (24) Biddinger, E. J.; Deak, D. V.; Ozkan, U. S. *Top. Catal.* **2009**, *52*,
921 1566.
- 922 (25) Zhang, L. P.; Xia, Z. H. *J. Phys. Chem. C* **2011**, *115*, 11170.
- 923 (26) Groves, M. N.; Chan, A. S. W.; Malardier-Jugroot, C.; Jugroot,
924 M. *Chem. Phys. Lett.* **2009**, *481*, 214.
- 925 (27) Lherbier, A.; Blase, X.; Niquet, Y. M.; Triozon, F.; Roche, S.
926 *Phys. Rev. Lett.* **2008**, *101*, 036808.
- 927 (28) Wu, M.; Cao, C.; Jiang, J. Z. *Nanotechnology* **2010**, *21*, 505202.
- 928 (29) Deifallah, M.; McMillan, P. F.; Corà, F. *J. Phys. Chem. C* **2008**,
929 *112*, 5447.
- 930 (30) Wei, D.; Liu, Y.; Wang, Y.; Zhang, H.; Huang, L.; Yu, G. *Nano*
931 Lett. **2009**, *9*, 1752.
- 932 (31) Wang, X.; Li, X.; Zhang, L.; Yoon, Y.; Weber, P. K.; Wang, H.;
933 Guo, J.; Dai, H. *Science* **2009**, *324*, 768.
- 934 (32) Huang, X.; Yin, Z.; Wu, S.; Qi, X.; He, Q.; Zhang, Q.; Yan, Q.;
935 Boey, F.; Zhang, H. *Small* **2011**, *7*, 1876.
- 936 (33) Guo, S.; Dong, S. *Chem. Soc. Rev.* **2011**, *40*, 2644.
- 937 (34) Wei, D.; Liu, Y. *Adv. Mater.* **2010**, *22*, 3225.
- 938 (35) Liu, H.; Liu, Y.; Zhu, D. *J. Mater. Chem.* **2011**, *21*, 3335.
- 939 (36) Reina, A.; Jia, X. T.; Ho, J.; Nezich, D.; Son, H.; Bulovic, V.;
940 Dresselhaus, M. S.; Kong, J. *Nano Lett.* **2009**, *9*, 30.
- 941 (37) Zhang, J.; Zou, H.; Qing, Q.; Yang, Y.; Li, Q.; Liu, Z.; Guo, X.;
942 Du, Z. *J. Phys. Chem. B* **2003**, *107*, 3712.
- 943 (38) Che, G.; Lakshmi, B. B.; Martin, C. R.; Fisher, E. R.; Ruoff, R. S.
944 *Chem. Mater.* **1998**, *10*, 260.
- 945 (39) Maldonado, S.; Morin, S.; Stevenson, K. J. *Carbon* **2006**, *44*,
946 1429.
- 947 (40) Luo, Z.; Lim, S.; Tian, Z.; Shang, J.; Lai, L.; MacDonald, B.; Fu,
948 C.; Shen, Z.; Yu, T.; Lin, J. *J. Mater. Chem.* **2011**, *21*, 8038.
- 949 (41) Qu, L.; Liu, Y.; Baek, J. B.; Dai, L. *ACS Nano* **2010**, *4*, 1321.
- 950 (42) Di, C. A.; Wei, D.; Yu, G.; Liu, Y.; Guo, Y.; Zhu, D. *Adv. Mater.*
951 **2008**, *20*, 3289.
- 952 (43) Reddy, A. L. M.; Srivastava, A.; Gowda, S. R.; Gullapalli, H.;
953 Dubey, M.; Ajayan, P. M. *ACS Nano* **2010**, *4*, 6337.
- 954 (44) Jin, Z.; Yao, J.; Kittrell, C.; Tour, J. M. *ACS Nano* **2011**, *5*, 4112.
- 955 (45) Imamura, G.; Saiki, K. *J. Phys. Chem. C* **2011**, *115*, 10000.
- 956 (46) Cho, Y. J.; Kim, H. S.; Baik, S. Y.; Myung, Y.; Jung, C. S.; Kim,
957 C. H.; Park, J.; Kang, H. S. *J. Phys. Chem. C* **2011**, *115*, 3737.
- 958 (47) Kudashov, A. G.; Okotrub, A. V.; Bulusheva, L. G.; Asanov, I. P.;
959 Shubin, Y. V.; Yudanov, N. F.; Yudanova, L. I.; Danilovich, V. S.;
960 Abrosimov, O. G. *J. Phys. Chem. B* **2004**, *108*, 9048.
- 961 (48) Liu, J.; Webster, S.; Carroll, D. L. *J. Phys. Chem. B* **2005**, *109*,
962 15769.
- 963 (49) Lv, W. X.; Zhang, R.; Xia, T. L.; Bi, H. M.; Shi, K. Y. *J. Nanopart.*
964 Res. **2011**, *13*, 2351.
- 965 (50) Zhang, C.; Fu, L.; Liu, N.; Liu, M.; Wang, Y.; Liu, Z. *Adv. Mater.*
966 **2011**, *23*, 1020.
- 967 (51) Choucair, M.; Thordarson, P.; Stride, J. A. *Nat. Nanotechnol.* **968**
2009, *4*, 30.
- 969 (52) Deng, D.; Pan, X.; Yu, L.; Cui, Y.; Jiang, Y.; Qi, J.; Li, W. X.; Fu,
970 Q.; Ma, X.; Xue, Q.; Sun, G.; Bao, X. *Chem. Mater.* **2011**, *23*, 1188.
- 971 (53) Droppa, R.; Hammer, P.; Carvalho, A. C. M.; dos Santos, M. C.;
972 Alvarez, F. *J. Non-Cryst. Solids* **2002**, *299*–302, 874.
- 973 (54) Journet, C.; Maser, W. K.; Bernier, P.; Loiseau, A.; Lamy de la
974 Chapelle, M.; Lefrant, S.; Deniard, P.; Lee, R.; Fischer, J. E. *Nature* **975**
1997, *388*, 756.
- 976 (55) Suenaga, K.; Colliex, C.; Demonty, N.; Loiseau, A.; Pascard, H.;
977 Willaime, F. *Science* **1997**, *278*, 653.
- 978 (56) Panchakarla, L. S.; Subrahmanyam, K. S.; Saha, S. K.;
979 Govindaraj, A.; Krishnamurthy, H. R.; Waghmare, U. V.; Rao, C. N. *R. Adv. Mater.* **980**
2009, *21*, 4726.
- 981 (57) Ghosh, A.; Late, D. J.; Panchakarla, L. S.; Govindaraj, A.; Rao, C.
982 N. R. *J. Exp. Nanosci.* **2009**, *4*, 313.
- 983 (58) Subrahmanyam, K. S.; Panchakarla, L. S.; Govindaraj, A.; Rao,
984 C. N. R. *J. Phys. Chem. C* **2009**, *113*, 4257.
- 985 (59) Guo, B.; Liu, Q.; Chen, E.; Zhu, H.; Fang, L.; Gong, J. R. *Nano*
986 Lett. **2010**, *10*, 4975.
- 987 (60) Geng, D.; Chen, Y.; Chen, Y.; Li, Y.; Li, R.; Sun, X.; Ye, S.;
988 Knights, S. *Energy Environ. Sci.* **2011**, *4*, 760.
- 989 (61) Kinoshita, K. *Carbon: Electrochemical and Physicochemical*
990 Properties; Wiley: New York, 1988.
- 991 (62) Sheng, Z. H.; Shao, L.; Chen, J. J.; Bao, W. J.; Wang, F. B.; Xia,
992 X. H. *ACS Nano* **2011**, *5*, 4350.
- 993 (63) Li, X.; Wang, H.; Robinson, J. T.; Sanchez, H.; Diankov, G.; Dai,
994 H. J. *Am. Chem. Soc.* **2009**, *131*, 15939.
- 995 (64) Golberg, D.; Bando, Y.; Bourgeois, L.; Kurashima, K.; Sato, T.
996 *Carbon* **2000**, *38*, 2017.
- 997 (65) Morant, C.; Andrey, J.; Prieto, P.; Mendiola, D.; Sanz, J. M.;
998 Elizalde, E. *Phys. Status Solidi A* **2006**, *203*, 1069.
- 999 (66) Suenaga, K.; Johansson, M. P.; Hellgren, N.; Broitman, E.;
1000 Wallenberg, L. R.; Colliex, C.; Sundgren, J. E.; Hultman, L. *Chem. Phys.*
1001 Lett. **1999**, *300*, 695.
- 1002 (67) Imran Jafri, R.; Rajalakshmi, N.; Ramaprabhu, S. *J. Mater. Chem.*
1003 **2010**, *20*, 7114.
- 1004 (68) Wang, Y.; Shao, Y.; Matson, D. W.; Li, J.; Lin, Y. *ACS Nano*
1005 **2010**, *4*, 1790.
- 1006 (69) Jeong, H. M.; Lee, J. W.; Shin, W. H.; Choi, Y. J.; Shin, H. J.;
1007 Kang, J. K.; Choi, J. W. *Nano Lett.* **2011**, *11*, 2472.
- 1008 (70) Lin, Y. C.; Lin, C. Y.; Chiu, P. W. *Appl. Phys. Lett.* **2010**, *96*,
1009 133110.
- 1010 (71) Long, D.; Li, W.; Ling, L.; Miyawaki, J.; Mochida, I.; Yoon, S. H.
1011 *Langmuir* **2010**, *26*, 16096.
- 1012 (72) Wang, D. W.; Gentle, I. R.; Lu, G. Q. *Electrochim. Commun.* **1013**
2010, *12*, 1423.
- 1014 (73) Zhang, L. S.; Liang, X. Q.; Song, W. G.; Wu, Z. Y. *Phys. Chem.*
1015 *Chem. Phys.* **2010**, *12*, 12055.
- 1016 (74) Cançado, L. G.; Pimenta, M. A.; Neves, B. R. A.; Dantas, M. S.;
1017 S.; Jorio, A. *Phys. Rev. Lett.* **2004**, *93*, 247401.
- 1018 (75) Dresselhaus, M. S.; Dresselhaus, G.; Saito, R.; Jorio, A. *Phys. Rep.*
1019 **2005**, *409*, 47.
- 1020 (76) Ferrari, A. C.; Meyer, J. C.; Scardaci, V.; Casiraghi, C.; Lazzari,
1021 M.; Mauri, F.; Piscanec, S.; Jiang, D.; Novoselov, K. S.; Roth, S.; Geim,
1022 A. K. *Phys. Rev. Lett.* **2006**, *97*, 187401.
- 1023 (77) Tuinstra, F.; Koenig, J. L. *J. Chem. Phys.* **1970**, *53*, 1126.
- 1024 (78) Nemanich, R. J.; Solin, S. A. *Phys. Rev. B* **1979**, *20*, 392.
- 1025

- 1026 (79) Cançado, L. G.; Takai, K.; Enoki, T.; Endo, M.; Kim, Y. A.;
1027 Mizusaki, H.; Jorio, A.; Coelho, L. N.; Magalhães-Paniago, R.; Pimenta,
1028 M. A. *Appl. Phys. Lett.* **2006**, *88*, 163106.
- 1029 (80) Das, A.; Pisana, S.; Chakraborty, B.; Piscanec, S.; Saha, S. K.;
1030 Waghmare, U. V.; Novoselov, K. S.; Krishnamurthy, H. R.; Geim, A.
1031 K.; Ferrari, A. C.; Sood, A. K. *Nat. Nanotechnol.* **2008**, *3*, 210.
- 1032 (81) Ni, Z. H.; Wang, H. M.; Kasim, J.; Fan, H. M.; Yu, T.; Wu, Y.
1033 H.; Feng, Y. P.; Shen, Z. X. *Nano Lett.* **2007**, *7*, 2758.
- 1034 (82) Graf, D.; Molitor, F.; Ensslin, K.; Stampfer, C.; Jungen, A.;
1035 Hierold, C.; Wirtz, L. *Nano Lett.* **2007**, *7*, 238.
- 1036 (83) Wu, Y. H.; Yu, T.; Shen, Z. X. *J. Appl. Phys.* **2010**, *108*, 071301.
- 1037 (84) Zhao, L.; He, R.; Rim, K. T.; Schiros, T.; Kim, K. S.; Zhou, H.;
1038 Gutiérrez, C.; Chockalingam, S. P.; Arguello, C. J.; Pálová, L.;
1039 Nordlund, D.; Hybertsen, M. S.; Reichman, D. R.; Heinz, T. F.; Kim,
1040 P.; Pinczuk, A.; Flynn, G. W.; Pasupathy, A. N. *Science* **2011**, *333*, 999.
- 1041 (85) Casiraghi, C.; Pisana, S.; Novoselov, K. S.; Geim, A. K.; Ferrari,
1042 A. C. *Appl. Phys. Lett.* **2007**, *91*, 233108.
- 1043 (86) Gupta, A.; Chen, G.; Joshi, P.; Tadigadapa, S.; Eklund, P. C.
1044 *Nano Lett.* **2006**, *6*, 2667.
- 1045 (87) Ferrari, A. C. *Solid State Commun.* **2007**, *143*, 47.
- 1046 (88) Herz, M.; Giessibl, F. J.; Mannhart, J. *Phys. Rev. B* **2003**, *68*,
1047 045301.
- 1048 (89) Zheng, B.; Hermet, P.; Henrard, L. *ACS Nano* **2010**, *4*, 4165.
- 1049 (90) Yu, Y. L.; Hu, Y. P.; Liu, X.; Deng, W. Q.; Wang, X. *Electrochim.
1050 Acta* **2009**, *54*, 3092.
- 1051 (91) Sun, S.; Murray, C. B.; Weller, D.; Folks, L.; Moser, A. *Science
1052* **2000**, *287*, 1989.
- 1053 (92) Kristian, N.; Yan, Y. S.; Wang, X. *Chem. Commun.* **2008**, 353.
- 1054 (93) Kristian, N.; Yu, Y. L.; Gunawan, P.; Xu, R.; Deng, W. Q.; Liu,
1055 X. W.; Wang, X. *Electrochim. Acta* **2009**, *54*, 4916.
- 1056 (94) Wang, Y.; Nguyen, T.; Liu, X.; Wang, X. *J. Power Sources* **2010**,
1057 *195*, 2619.
- 1058 (95) Aihara, J. I. *J. Phys. Chem. A* **1999**, *103*, 7487.
- 1059 (96) Kurak, K. A.; Anderson, A. B. *J. Phys. Chem. C* **2009**, *113*, 6730.
- 1060 (97) Huang, S. F.; Terakura, K.; Ozaki, T.; Ikeda, T.; Boero, M.;
1061 Oshima, M.; Ozaki, J. I.; Miyata, S. *Phys. Rev. B* **2009**, *80*, 235410.
- 1062 (98) Yu, L.; Pan, X.; Cao, X.; Hu, P.; Bao, X. *J. Catal.* **2011**, *282*, 183.
- 1063 (99) Paulus, U. A.; Schmidt, T. J.; Gasteiger, H. A.; Behm, R. J. *J.
1064 Electroanal. Chem.* **2001**, *495*, 134.
- 1065 (100) Nagaiah, T. C.; Kundu, S.; Bron, M.; Muhler, M.; Schuhmann,
1066 W. *Electrochim. Commun.* **2010**, *12*, 338.
- 1067 (101) Niwa, H.; Horiba, K.; Harada, Y.; Oshima, M.; Ikeda, T.;
1068 Terakura, K.; Ozaki, J. I.; Miyata, S. *J. Power Sources* **2009**, *187*, 93.
- 1069 (102) Okamoto, Y. *Appl. Surf. Sci.* **2009**, *256*, 335.
- 1070 (103) Tsai, C. W.; Tu, M. H.; Chen, C.-J.; Hung, T. F.; Liu, R. S.;
1071 Liu, W. R.; Lo, M. Y.; Peng, Y. M.; Zhang, L.; Zhang, J.; Shy, D. S.;
1072 Xing, X. K. *RSC Adv.* **2011**, *1*, 1349.
- 1073 (104) Liang, Y.; Li, Y.; Wang, H.; Zhou, J.; Wang, J.; Regier, T.; Dai,
1074 H. *Nat. Mater.* **2011**, *10*, 780.
- 1075 (105) Avouris, P.; Chen, Z.; Perebeinos, V. *Nat. Nanotechnol.* **2007**,
1076 *2*, 605.
- 1077 (106) Schwierz, F. *Nat. Nanotechnol.* **2010**, *5*, 487.
- 1078 (107) Wei, X. L.; Fang, H.; Wang, R. Z.; Chen, Y. P.; Zhong, J. X.
1079 *Appl. Phys. Lett.* **2011**, *99*, 012107.
- 1080 (108) Son, Y. W.; Cohen, M. L.; Louie, S. G. *Phys. Rev. Lett.* **2006**, *97*,
1081 216803.
- 1082 (109) Yu, S. S.; Zheng, W. T.; Wen, Q. B.; Jiang, Q. *Carbon* **2008**, *46*,
1083 537.
- 1084 (110) Li, Y.; Zhou, Z.; Shen, P.; Chen, Z. *ACS Nano* **2009**, *3*, 1952.
- 1085 (111) Biel, B.; Blase, X.; Triozon, F.; Roche, S. *Phys. Rev. Lett.* **2009**,
1086 *102*, 096803.
- 1087 (112) Perebeinos, V.; Tersoff, J.; Avouris, P. *Phys. Rev. Lett.* **2005**, *94*,
1088 027402.
- 1089 (113) Zhou, X.; Park, J. Y.; Huang, S.; Liu, J.; McEuen, P. L. *Phys.
1090 Rev. Lett.* **2005**, *95*, 146805.
- 1091 (114) Pan, D.; Wang, S.; Zhao, B.; Wu, M.; Zhang, H.; Wang, Y.;
1092 Jiao, Z. *Chem. Mater.* **2009**, *21*, 3136.
- 1093 (115) Wu, Z. S.; Ren, W.; Xu, L.; Li, F.; Cheng, H. M. *ACS Nano*
1094 **2011**, *5*, 5463.
- (116) Wang, H.; Zhang, C.; Liu, Z.; Wang, L.; Han, P.; Xu, H.; 1095
Zhang, K.; Dong, S.; Yao, J.; Cui, G. *J. Mater. Chem.* **2011**, *21*, 5430. 1096
- (117) Cho, Y. J.; Kim, H. S.; Im, H.; Myung, Y.; Jung, G. B.; Lee, C. 1097
W.; Park, J.; Park, M. H.; Cho, J.; Kang, H. S. *J. Phys. Chem. C* **2011**, 1098
115, 9451. 1099
- (118) Jia, L.; Wang, D. H.; Huang, Y. X.; Xu, A. W.; Yu, H. Q. *J. Phys.
1100 Chem. C* **2011**, *115*, 11466. 1101